Welding between aluminum alloy and steel sheets by using transition joints

Welding between aluminum alloy and steel sheets by using transition joints

P. Matteis[1,*], A. Gullino[1], F. D'Aiuto[2], C. M. Puro[3], G. Scavino[1]

[1]Politecnico di Torino (Turin Technical University), DISAT dep., It-10129 Torino, Italy.

[2]formerly with Centro Ricerche FIAT (FIAT Research Center), GML dep., It-10135 Torino, Italy, is now with CBMM Europe BV, 1077 XV, Amsterdam, Netherlands

[3]Centro Ricerche FIAT (FIAT Research Center), GML dep., It-10135 Torino, Italy.

* Corresponding author.

Published in the *Journal of Materials Engineering and Performance* on Feb 3, 2020.

DOI: 10.1007/s11665-020-04595-2

ABSTRACT

Hybrid car bodies can be used to exploit the comparative advantages of steels and aluminum alloys for car lightweighting. This development hinges on the deployment of effective hybrid joining technologies. Hybrid welding with transition joints between 1.35 mm thick DP1000 dual-phase steel sheets and 2.5 mm thick 6106 aluminum alloy sheets is here investigated. The transition joints are fabricated by explosion welding, with a titanium interlayer. The aluminum alloy sheet, the transition joint, and the steel sheet are butt joined by arc welding, with appropriate fillers. The overall tensile strength of the hybrid joint is about 2/3 of the tensile strength of the homologous arc-welded joint fabricated by using the same aluminum alloy sheet, and it is not significantly affected by corrosion in still synthetic seawater.

1. Introduction

Due to ever more stringent regulation on carbon dioxide emissions and fuel economy, car manufacturers are trying new ways to decrease the car-body weight, without loss of performance and avoiding excessive cost. One possibility is the introduction of hybrid car bodies, whereby parts made with different materials, and especially with steels and aluminum alloys, are joined together [1,2].

Hybrid construction allows to decrease the car-body weight at a moderate cost, by using aluminum alloys only where they can achieve the maximum benefit. Moreover, it can be more effective than

full aluminum alloy construction as it regards the total carbon footprint, because it allows to use aluminum only where the weight reduction and the ensuing lower tailpipe emissions are sufficient to offset the much higher energy consumption and pollution that are associated with the production of aluminum alloys, in respect to steels.

Car bodies are usually built by joining several parts, which in turn are manufactured by sheet metal forming (deep drawing or hot-stamping), starting from steel or aluminum alloy sheets. Taylor welded blanks (TWB) are manufactured by joining several (often dissimilar) metal sheets on their edges and are also commonly employed as an input for the same sheet metal forming operations.

Therefore, the development of hybrid car bodies depends upon the deployment of effective technologies for joining steel sheets to aluminum alloy sheets, for both TWB manufacturing and final assembly of already formed parts. Some of these technologies were not previously used in the car sector and must be adapted to its requirement.

Currently, the most common hybrid joining technologies in the car industry, for the steel / aluminum alloy couple, are mechanical joining (e.g.: riveting, clinching, etc.) and adhesive bonding [3-5]. Nevertheless, several hybrid welding technologies allow to form a direct metallic bond between steel and aluminum alloy sheets [6], achieving a much higher strength per unit area than mechanical or adhesive joining, and have been used in the car industry in a few cases so far [7-9].

The main difficulty of hybrid welding technologies is the formation of brittle inter-metallic compounds (IMCs), e.g. Al_2Fe, Al_5Fe_2 and $Al_{13}Fe_4$ (or Al_3Fe) [6,10]. Therefore, the effectiveness of hybrid welding methods is especially (but not exclusively) related to their ability to avoid or minimize the formation of IMCs. In particular, solid-state welding technologies are especially suitable for hybrid welding, because the limited temperature increase and the absence of liquid metal hinder the development of IMCs [6].

Explosion welding is a well established solid welding process, which is commonly applied to dissimilar metal couples. In this process, a “flyer” metal sheet is accelerated by an explosion, and collides at high speed on a “parent” metal sheet, cleaning the faying surfaces from any oxides and contaminants and allowing the metallic bond [11].

Unfortunately, explosive welding cannot be applied in the car industry, because of geometrical limitations and of safety concern on the use of explosives. However, prefabricated steel - aluminum transition joints have been employed for a long time in the shipbuilding industry. These joint are bimetallic strips, which are cut from large explosion-welded clad plates, perpendicularly to the welding plane. They are mounted in between the steel hull or deck and the aluminum alloy superstructure, and are conventionally welded on both sides [12].

In the explosion welding process, a metallic interlayer is often placed between the aluminum and steel plates in order to improve the weldability and minimize the formation of IMCs. The interlayer

is explosion-welded with the aluminum alloy plate on one side and the steel plate on the other side. Usually, ductile materials such as 1000-series aluminum alloy, titanium or tantalum, are used as interlayer, allowing a high deformation during the explosion [13,14].

In some cases, the interlayer is also useful in order to avoid the formation of IMCs during the heating caused by the subsequent conventional welding processes performed on the two sides of the transition joint [13-15]. In particular, a titanium interlayer prevents the formation of the above mentioned brittle Al-Fe IMCs. In contrast, IMCs formed in the Al-Ti system are less harmful for mechanical properties of the joint, and are formed only after a longer time or at an higher temperature than the Al-Fe ones [16]. Moreover, a three-layer clad plate with a titanium interlayer can be fabricated in one explosion [16], whereas other types of three-layer plates require two separate explosions, one for each welded interface, making them more expensive.

Commercially available transition joints between steel and aluminum alloys with a titanium interlayer offer a tensile strength of 220 MPa or more, and can retain a tensile strength of 140 MPa or more after 24 h at 550 °C [17]. However, even if they are well established in other industries, explosion-welded transition joints are not currently used in the car industry.

An effective transition joint must allow a large distance between the bimetallic interface and the subsequent fusion welding lines, to prevent overheating of the bimetallic interface, and of the aluminum alloy itself, during the same fusion-welding operations, and especially during the steel fusion welding. Therefore, if the transition joint is cut from a clad plate, the total plate thickness must be relatively large, e.g. of the order of 50 mm.

The latter minimum thickness condition can be easily met by the current explosion welding techniques, whereas it is more challenging for other solid-state welding techniques. In particular, it is well known that bimetallic clad sheets can be fabricated by roll bonding [6], and this route have also been proposed a long time ago for the fabrication of transition joints [18], but it has never become commonplace. This is probably because, on the one hand, the production of thick clad plate by roll bonding requires an even greater thickness at the start of the rolling process, and, on the other hand, the rolling temperature must be relatively low, at least for the steel side (to avoid overheating of the interface and the aluminum alloy side); therefore the initial rolling force would be very large and for this reason the process would be expensive. In fact, the current production of roll-bonded clad sheets is generally restricted to a total thickness of less than 5 mm [18,19]. In principle, special transition-joint geometries (in which the bimetallic interface is not perpendicular to the plane that contains the two fusion-welding lines) could be used to overcome this limitation [6,18], but this approach have not been demonstrated as yet [6].

A further advantage of the use of transition joints obtained from clad plates is that, contrary to several other joining methods, the eventual hybrid joint does not exhibit any bimetallic crevice, which is desiderable from the point of view of corrosion resistance.

Thus, the possible use of explosion-welded transition joints in the automotive sector, especially for car-body applications, was investigated and is reported here. For this purpose, a high-strength steel sheet and an aluminum alloy sheet for car-body application have been welded by using a bimetallic strip, or transition joint, which in turn had been manufactured by cutting a clad plate, which was made by explosion welding by using a titanium interlayer. Transition joints fabricated by roll bonding with special geometries were also investigated and will be reported separately.

Welding between each side of the transition joint and the corresponding metal sheet has been performed by Gas Metal Arc Welding (GMAW). This technique allows to fabricate a continuous linear joint and is well established in the car industry. By using appropriate gases and filler wires, arc welding has been successfully applied to dissimilar steel couples for car-body applications [20,21]. In particular, a pulsed GMAW technique was chosen here because, in respect to conventional GMAW, it achieves a lower heat input and hence a better performance on heat-treatable aluminum alloys [22,23].

2. Materials and methods

2.1 Metal sheets

The examined base materials were a DP1000 dual phase steel sheet, equivalent to the European grade HCT980X [24], 1.35 mm thick, coated with zinc alloy for corrosion protection on both sides, and a 6106 (Mg-Si) aluminum alloy sheet [25], 2.5 mm thick, uncoated. The examined steel sheets originated from two nominally equal batches, which are here called batch I and II and are considered equivalent. The base materials were investigated by Atomic Emission Spectroscopy with spark excitation (spark-AES), optical metallography and microhardness testing (with load 0.1 Kg).

2.2 Homologous arc-welding tests

The homologous welding tests were performed by using the TPS 4000 CMT arc-welding system, together with the VR 7000 CMT wire feed system and the RCU 5000i control unit, all manufactured by Fronius (Pettenbach, Austria).

Gas Metal Arc welding was performed by using a consumable filler wire, with a pulsed-arc method, also known with the "CMT" or "Cold Metal Transfer" trade name. In this method, the arc length is mechanically controlled by pushing or pulling the wire (with a dedicated device in the torch) and

the arc length, current and tension are modified cyclically in order to deposit one filler droplet in every cycle with the lowest possible heat input [23,26].

In the homologous steel welding tests (which were performed on steel batch I), the active welding gas was a mixture containing 82 vol.% CO_2 and 18 vol.% O_2 and the filler wire was G 3Si1 [27], with the following nominal composition: 0.06 - 0.14 wt.% C, 0.7 - 1 wt.% Si, 1.3 - 1.6 wt.% Mn. In the aluminum alloy welding tests, the inert welding gas was Ar and the filler wire was S Al 4043 [28], with nominal composition: 11 - 13 wt.% Si. The diameter of the filler wires was 1.2 mm in all cases. The instantaneous wire speed was automatically controlled so as to achieve the preset mean value (or wire feed rate). The arc current and tension were also continuously and automatically modified by the control system and an approximate overall mean values was recorded for each weld. The preset mean wire speed and the mean arc current and arc tension values are given in table I.

All welding tests were performed in the butt welding configuration. The length of the faying edges was 200 mm, and the length of the weld seam was at least 120 mm. The base metal sheets were clamped horizontally on a steel support plate and the welding torch acted from above. The welding torch was driven at constant speed along the horizontal linear weld path by using a robotic arm guided by an independent control system (model Smart S2, manufactured by Comau, Torino, Italy). The preset torch speed values are also reported in table I.

2.3 Transition joints

The examined transition joints were manufactured by cutting a three-layer clad plate, which in turn had been manufactured by explosion welding by NobelClad Europe SAS (Perpignan, France).

In the as-received condition, the three layers of the clad plate were as follow: a 37.4 mm thick base layer of SAE/AISI 1008 low-carbon steel; a 1.3 mm thick interlayer of commercially pure, grade 1 titanium; and a 12.3 mm thick clad layer of 3003 aluminum alloy (with small local variations in the layers thickness), as shown in figure 1a.

The three alloys used in the clad plate were chosen for the following reasons. In the first place, as noted above in the introduction section, the titanium interlayer prevents the formation of IMCs during subsequent heating, thus allowing to perform the ensuing arc-welding operations at relatively close distance from the original explosion-welded interface. In the second place, the 3003 aluminum alloy and the titanium grade one alloy have sufficient ductility to act as flyer plates in the explosion welding process, whereas other less ductile alloys could not be used for this purpose. In the third place, prior industrial experience [17] has demonstrated that the 3003 aluminum alloy can be reliably explosion-welded to the titanium interlayer, whereas other aluminum alloys, including the Al-Mg alloys that are commonly used in other types of transition joints for shipbuilding, are not

compatible with the same titanium interlayer [29]. Finally, this particular combination of alloys is well established, implying that all relevant explosion welding parameters are well known and the clad plate could be produced without effort. On the contrary, there were no strict requirements on the choice of the steel grade. In fact, the steel plate is the base plate in the explosion welding process, and therefore it is subjected to less stringent ductility requirements than the flier plates; furthermore, the transversal strength of the transition joint is practically unaffected by the strength of the steel side, as far as it is greater than the strength of the 3003 aluminum alloy - which is a very low requirement for any steel. Therefore, the 1008 steel grade was chosen for its availability and weldability.

The thickness of the steel and aluminum alloy layers of the clad plate is equal to the maximum distance between the original explosion-welded bimetallic interfaces and the ensuing arc-welding lines; therefore a relatively large thickness was chosen for both sides to prevent the overheating of the bimetallic interfaces during the arc welding, and the steel side was designed to be ticker than the aluminum alloy side because the maximum expected temperature during arc-welding is higher on the steel side than on the aluminum alloy side.

The as-received clad plate was examined by optical metallography and microhardness testing (with load 0.1 Kg). Moreover, small specimens obtained from the same clad plate were heat-treated at 550 °C for up to 24 h, and were then similarly examined by optical metallography. The latter test was performed to verify if IMCs could be formed on the bimetallic interfaces as a consequence of heating, by investigating the most severe heating possible, short of the incipient melting of the aluminum alloy.

The as-received clad plate was then cut (by using abrasive cutting wheels) into 2.8 mm thick slices, perpendicular to the welded planes, which are hereafter called transition joints (figure 1).

2.4 Hybrid arc-welding tests

The 1.35 mm thick DP1000 steel sheet samples, the 2.8 mm thick transition joints, and the 2.5 mm thick 6106 (Si-Mg) aluminum alloy sheet samples were joined with two homologous arc-welding seams, performed between the steel sheet and the steel side of the transition joint, and between the aluminum alloy sheet and the aluminum alloy side of the transition joint, respectively, as shown in figure 2a and 2b.

The welding beads on the steel and aluminum alloy sides were done separately (one after the other) and each type of weld was generally performed in the same way as described above for the homologous welding tests, but the wire and torch speed and the arc current and tension were modified and are reported in table I.

In particular, as it regards the steel side, the wire speed and arc current were increased, in respect to the homologous welding test, because the transition joint was thicker than the steel sheet, and were equal for all hybrid joints, as reported in table I. The steel batch used for each type of test is also listed in table I.

In contrast, as it regards the Al alloy side, different values of the wire and torch speed and of the arc current and tension were investigated, and are here reported as type A, B and C hybrid joints, as specified in table I.

The butt welding setup and geometry were also generally the same as described above for the homologous welding tests, with the partial exception of the type C hybrid joints, in which both sides were clamped upon 0.75 mm thick steel sheet pieces, in turn laying on the same support plate, so as to leave a 0.75 mm gap between the lower edges of the faying surfaces and the support plate. Both welding setups are illustrated in figure 3, in the case of the aluminum alloy side weld.

Some partial hybrid joints, in which only one side of the transition joint was welded with its corresponding metal sheet, were also performed and used for metallographic examination.

2.5 Characterization of the welded joints

After welding, several (up to five) 25 mm wide transversal tensile specimens were contour-cut from the central portion of each homologous or hybrid joint, excluding the two ends of the weld seam, by means of an abrasive water jet, as shown inure 2c. During this operation, the original sheet surfaces and weld bead surfaces were not modified. The total length of the tensile specimens was about 250 mm.

Tensile specimens obtained from both homologous and hybrid joints were submitted to tensile testing in the as-fabricated condition. Moreover, further tensile specimens obtained from the hybrid joints were submitted first to free corrosion for 3 weeks, and then to tensile testing.

The free corrosion tests were performed by full immersion in still synthetic seawater, which in turn was prepared by adding 3.5 wt.% reagent-grade NaCl into distilled water, and were generally compliant to the ISO 11845 guidelines [30,31].

All tensile tests were performed under actuator displacement control at the constant speed of 0.1 mm/s. The stress was calculated as the force divided by the initial cross section of the metal sheets; for hybrid joints, the initial cross section of the Al alloy sheet was used, in order to facilitate the comparison with the mechanical properties of the weakest metal sheet. Moreover, the axial lengths of the steel and Al alloy sides of the transition joint were measured after the tests (by fitting together the broken pieces if necessary). All other aspects of the tensile tests were generally compliant to the ISO 4136 an/or ISO 6892-1 standards [32,33].After the tensile tests, the fracture surfaces of

selected tensile specimens (both as-welded and corroded) were examined by Scanning Electron Microscopy (SEM).

Furthermore, smaller transversal specimens were also cut from the welded joints, and employed to perform optic and electronic metallographic observations, energy dispersion spectroscopy (EDS) analyses, and microhardness tests (with load 0.1 Kg). The metallographic preparation procedures were generally compliant to the ASTM E3 and ASTM E407 guidelines [34,35], and the microhardness tests were compliant to the ISO 6507 standard [36].

3. Results and discussion

3.1 Metallurgical properties of as-received materials

The elemental composition of the examined materials is listed in tables II and III. The elemental composition of the DP1000 and 6106 base metals was obtained by spark-AES, whereas the elemental composition of the aluminum alloy and steel layers of the clad plate is the heat analysis given by their respective suppliers.

The microstructure of the base metals, as revealed by standard optical metallography, is shown in figure 4. In the as-received dual phase steel, figure 4a, the martensite volume fraction is about 7 % and the ferrite grain size is about 30 μm. The microhardness is about 316 HV0.1. The aluminum alloy microstructure exhibits primary and secondary precipitates, formed during casting and ingot annealing, and some fine precipitates (the grain boundaries were not revealed by the Keller etching, figure 4b). The microhardness is about 67 HV0.1.

The three-layered, explosion welded clad plate was examined both in the as-received condition and after heating at 550°C for up to 24 h (figures 5 and 6).

In the as-received condition, the microstructure of the steel layer is ferrite and pearlite, and the microhardness of the Al alloy, titanium and steel, close to the weld surfaces, is about 50, 230 and 145 HV, respectively (figure 6). Far away from the weld planes, both the aluminum alloy and steel layers show somewhat lower hardness (about 45 and 130 HV0.1, respectively), proving that the material close to the impact (weld) surfaces underwent strain hardening. Finally, after careful examination, no IMCs could be detected by means of optical microscopy on the two bimetallic interfaces (figure 5a,c).

After the 550 °C heat treatment, no significant modifications of the two bimetallic interface could be detected by optical microscopy; in particular, no newly formed IMCs were detected (figure 5b,d).

3.2 Metallurgical properties of welded joints

In the homologous arc-welded steel joints, the weld bead is about 6 mm wide and the Heat Affected Zone (HAZ) on each side of the weld bead is about 3 mm wide. The maximum hardness, about 430 HV0.1, is reached in the HAZ, where the microstructure consist of low-carbon martensite; on the contrary the weld bead is somewhat softer, about 340 HV, exhibiting a mixed microstructure with a significant amount of ferrite, probably because the carbon content of the filler metal was lower than that of the base metal.

In the homologous arc-welded aluminum joints, the weld bead is about 8 mm wide and it exhibits a dendritic microstructure with a dendritic cell size of about 8 μm, together with about 5 % diffuse porosity, consisting of circular closed pores with diameters up to 150 μm. This porosity level is significantly higher than those previously achieved with the pulsed-arc method on other aluminum alloy couples [23] and it probably derives from the absorption of hydrogen atoms (originating from ambient humidity or surface contamination) into the liquid metal and the ensuing development of hydrogen gas during the solidification of the weld bead [22].

Typical macroscopic cross sections of the welds between the transition joint and the two base metal sheets are shown in figure 7. The steel weld was sound and the HAZ was about 3 mm wide on the steel sheet side, and 2 mm wide on the transition joint side. The Al alloy weld showed up to 9 % porosity, with a pore morphology similar to that encountered in the homologous Al alloy welds.

The microstructure of the weld bead and HAZ and the overall microhardness profile of the steel side weld are shown in figures 8 and 9, respectively; those of the Al alloy side weld are shown in figures 10 and 11, respectively.

In the steel weld, the HAZ microstructure is ferritic-martensitic on the transition joint side (figure 8a), with hardness up to 185 HV (figure 9) and is fully martensitic on the sheet side (figure 8), with hardness up to 450 HV (figure 9). The hardness of the weld bead is about 250 HV (figure 9).

In the Al alloy weld, the maximum microhardness, about 80 HV (figure 11), is reached in the weld bead, which exhibits a dendritic microstructure, with a cell size of about 11 μm (figure 10a), and with silicon particles in the interdendritic regions, consistent with the composition of the Al-Si filler wire. The microhardness of the HAZ of the Al alloy size is not significantly modified in respect to the base metal, whereas the HAZ of the transition joint side is somewhat softened, about 37 HV (figure 11).

The explosion-welded interfaces of the transition joint were also examined by scanning electron microscopy (SEM) and by EDS, on a type B hybrid joint (figures 12 and 13). No IMCs were detected on either interface by SEM (figure 12), and only very limited interdiffusion could be detected within about 50 μm from the same interfaces by EDS (figure 12b and 13).

Since the heating of the original explosion-welded interfaces during the ensuing lateral welding operation is determined by the distance between the former and the latter welding planes, it can be

inferred that the width of the here employed transition joint (about 12 mm on the aluminum side and 37 mm on the steel side) was more than sufficient to avoid any thermal damage to the explosion-welded joint.

3.3 Corrosion behavior

After the 3-week seawater corrosion tests, the hybrid specimens showed different corrosion mechanisms in different parts of their surface (figure 14 and 15).

On the steel sheet, the zinc alloy layer was partially corroded, but there was little or no evidence of corrosion of the steel substrate. The steel weld bead was also itself largely unaffected by corrosion, retaining its original dark appearance (due to high-temperature oxidation during welding), but some red corrosion products (due to the corrosion of iron) were apparent on small areas within the HAZ of steel weld, especially on the transition joint side.

The bare steel side of the transition joint (far away from the welds) was also generally unaffected by corrosion. Local corrosion occurred near the explosion-welding planes, on both sides of the titanium interlayer (figure 15). Red corrosion products were evident close to the steel - titanium interface, evidencing the typical waviness of the same interface and especially the tips of the waves. Moreover, the aluminum side of the transition joint showed significant signs of corrosion, especially (but not only) near the titanium interlayer.

Finally, the aluminum sheet also showed evident corrosion, which was more intense close to aluminum-side weld bead.

These results are here attributed mainly to the electrical coupling between the steel parts, the zinc alloy coating, and the aluminum alloy parts, causing galvanic protection of the steel surfaces at the expense of the aluminum alloy and zinc alloy ones. The galvanic origin of the aluminum corrosion is further evidenced by the fact that aluminum is more deeply corroded close to the bimetallic interfaces than far away from them. However, the overall galvanic coupling between iron, zinc and aluminum does not explain the localized corrosion found on small areas of the steel surfaces. In particular, the localized steel corrosion near the explosion welded interface may be due to increased local reactivity caused by the intense local plastic deformation undergone during the explosion welding process; whereas the localized steel corrosion around the steel weld seam may be caused by local interaction with the iron oxide layers formed on the same weld seem at high temperature during the welding process.

3.4 Fracture mechanisms and tensile strength

The transversal tensile strength of the homologous and hybrid welded joints, both before and after the corrosion tests, is reported in table IV and in figure 16, and a set of tensile curves obtained on

the same type of hybrid joint, before and after the corrosion test, is reported in Figure 17. Typical fractured hybrid specimens are shown in figures 18 and 19, for the as-welded and corroded cases, respectively, and typical fracture surfaces of as-welded specimens are shown in figure 20 (those of corroded specimens were similar).

The mean transversal tensile strength of the homologous steel and aluminum alloy joints is about 763 and 206 MPa, respectively. Therefore, at least in the as-welded state, the aluminum alloy side was expected to be the weakest link of all examined hybrid joints (even if it was somewhat thicker than the steel side). In fact, all hybrid specimens, both as-welded and corroded, were broken at or close to the Al-alloy weld, usually either in the middle of the weld seam, or in the heat affected zone on the transition joint side, as shown in figures 18 and 19 for type C joints (only in one case the fracture occurred in part on the aluminum alloy / titanium interface).

The tensile fracture was generally ductile. The fracture surfaces of the specimens broken in the heat affected zone was formed entirely by microvoid coalescence, as shown in figure 20a and b. When the fracture occurred in the aluminum alloy weld seam, it was facilitated by porosity, as shown figure 20c and 20d, evidencing several pores on the fracture surface; the remaining part of the fracture surface was in these cases also formed by microvoids, which were mostly nucleated from the silicon particles. It has been demonstrated by prior work that the pore area fraction on the fracture surface of arc-welded aluminum alloy joints is negatively correlated with the joint strength [37,38]; therefore, it is likely that the strength of the specimens broken in the weld seam was significantly diminished due to the above noted porosity of the same weld seam.

The prevalent fracture locations, the overall appearance of the fracture surfaces, and the microscopic fracture mechanisms, were the same in both the as-welded and corroded specimens; therefore the failure mechanisms were not modified by the corrosion stage.

By measuring the axial length of the steel and aluminum alloy sides of the transition joint, it was found that the 3003 Al alloy side exhibits about 6 % permanent elongation in those specimens that were broken in the heat affected zone, whereas the Al alloy side of the specimens broken in the weld seam, as well as the steel side of all specimens, did not exhibit any appreciable permanent elongation, therefore they were probably loaded within their macroscopic elastic limit.

The transversal tensile strength of the as-welded hybrid joints is comprised between 54 % and 66 % of the tensile strength of the homologous Al alloy joints, the best result being achieved by the type B hybrid joints. The tensile strength of the hybrid joints was not detectably diminished by the 3-week seawater corrosion stage (table IV and figures 16 and 17); in fact, the differences due to the additional corrosion stage, if any, were smaller than the statistical data dispersion. Therefore, the abovementioned corrosion of the aluminum alloy surfaces either was too shallow to be consequential, or was much less influent than the variability of the aluminum weld bead. Moreover,

the local corrosion near the explosion-welding planes was also inconsequential, as the tensile fracture occurred elsewhere.

Overall, the lower transversal strength of the hybrid joint, in respect to the homologous aluminum-alloy welds, appears to derive entirely from the lower strength of the dissimilar weld between the 3003 and 6106 aluminum alloys, in respect to the homologous weld performed on the 6106 alloy. Since the strength of arc-welded aluminum alloy joints decreases by increasing the pore volume fraction [37-39], this difference can be in part traced back to the greater porosity of the aluminum alloy weld beads of the hybrid specimens, in respect to the homologous weld beads.

4. Conclusions

Hybrid welding between steel sheets and aluminum alloy sheets, by way of explosion-welded transition joints, was experimentally investigated here as a possible joining technology for the manufacturing of lightweight affordable hybrid car bodies. The transition joints were fabricated by explosion welding, with a titanium interlayer. The DP1000 steel sheet, the transition joint, and the 6106 aluminum alloy sheet were then butt joined by gas metal arc welding. Homologous steel and aluminum alloy welded joints were also fabricated for comparison. Results were assessed by means of metallographic examinations, corrosion tests, and transversal tensile tests.

The weld between the steel sheet and the steel side of the transition joint was free of macroscopic defects. The maximum hardness, about 450 HV, occurred in the heat affected zone of the steel sheet, where the microstructure was fully martensitic, whereas both the weld bead and the heat affected zone of the transition joint showed mixed microstructures with lower hardness.

The weld between the aluminum alloy sheet and the steel side of the transition joint showed up to 9 % porosity. The maximum hardness, about 80 HV, occurred in the weld bead, which exhibited a fine dendritic microstructure, whereas the hardness of the heat affected zone was almost unmodified on the sheet side, and somewhat decreased on the transition joint side.

The original explosion-welded interfaces of the transition joint were not detectably affected or damaged by the ensuing arc-welding procedures, performed on the two sides of the same transition joint (no intermetallic compounds, and only very limited interdiffusion, were detected), proving that the width of the here employed transition joint (about 12 mm on the aluminum side and 37 mm on the steel side) was more than sufficient, and that narrower transition joints could be investigated in the future.

After the 3-week seawater corrosion tests, the aluminum alloy side of the hybrid joints showed limited galvanic corrosion, especially near the titanium interlayer and near the weld bead between the transition joint and the aluminum alloy sheet.

All hybrid transversal tensile specimens were broken on or close to the aluminum alloy weld, which was the weakest link of all here examined hybrid joints. For this reason, the transversal strength of the hybrid joints is here compared with that of the aluminum alloy homologous joints.

The transversal tensile strength of the as-welded hybrid joints was comprised between 54 % and 66 % of the transversal tensile strength of the homologous Al alloy joints, depending on the welding parameters. Moreover, notwithstanding the above-mentioned corrosion damage, the transversal tensile strength of the hybrid joints was not detectably diminished by the 3-week seawater corrosion.

Overall, from the present results it can be inferred that hybrid butt joints between steel and aluminum alloy sheets for car-body applications, effected by using explosion welded transition joints, can achieve fair transversal strength, are not excessively sensitive to corrosion, and ultimately can be an effective mean to fabricate hybrid car bodies.

Acknowledgements

A. Riolo and A. D'Aprile contributed to this work during the preparation of their M.Sc dissertations, L. Piovano during the preparation of his B.Sc. dissertation, and J. Guilbard during his traineeship project, all at the Politecnico di Torino (Turin Technical University), Torino, Italy. D. Gautier (Nobelclad Europe SAS, Perpignan, France) contributed to this work with useful discussion on the explosion-welding process.

References

[1] Goede, M., Stehlin, M., Rafflenbeul, L., Kopp, G., Beeh, E. Super light car - lightweight construction thanks to a multi-material design and function integration. European Transport Research Review, 2009, 1 (1), 5.

[2] Joost, W.J. Reducing vehicle weight and improving US energy efficiency using integrated computational materials engineering. JOM (Journal of the Minerals, Metals and Materials Society), 2012, 64(9), 1032-1038.

[3] Barnes, T. A., Pashby, I. R. Joining techniques for aluminium spaceframes used in automobiles: part II - adhesive bonding and mechanical fasteners. Journal of Materials Processing Technology, 2000, 99.1-3: 72-79.

[4] Groche, P., Wohletz, S., Brenneis, M., Pabst, C., Resch, F. Joining by forming - a review on joint mechanisms, applications and future trends. Journal of Materials Processing Technology, 2014, 214(10), 1972-1994.

[5] He, X. A review of finite element analysis of adhesively bonded joints. International Journal of Adhesion and Adhesives, 2011, 31(4), 248-264.

[6] Gullino, A., Matteis, P., D'Aiuto, F. Review of aluminum-to-steel welding technologies for car-body applications. Metals, 2019, 9(3), 315.

[7] Ohhama, S., Hata, T., Yahaba, T., Kobayashi, T., Miyahara, T., Sayama, M. Application of an FSW continuous welding technology for steel and aluminum to an automotive subframe. SAE Technical Paper, 2013, No. 2013-01-0372.

[8] Huland, S., Moller, M., Franke, M., Vakalopoulos, T. The electrification of the Passat, the GTE. Viavision, July 2015, Verlag Rommerskirchen, Remagen, Germany.

[9] Visnic, B., GM prepping industry-first steel-to-aluminum welding process. Automotive Engineering, may 2016.

[10] Shah, L. H., Ishak, M. Review of research progress on aluminum–steel dissimilar welding. Materials and Manufacturing Processes, 2014, 29(8), 928-933.

[11] Findik, F. Recent developments in explosive welding. Materials and Design, 2011, 32(3), 1081-1093.

[12] Tricarico, L., Spina, R. Experimental investigation of laser beam welding of explosion-welded steel/aluminum structural transition joints. Materials and Design, 2010, 31(4), 1981-1992.

[13] Han, J. H., Ahn, J. P., Shin, M. C. Effect of interlayer thickness on shear deformation behavior of AA5083 aluminum alloy/SS41 steel plates manufactured by explosive welding. Journal of Materials Science, 2003, 38(1), 13-18.

[14] Aceves, S. M., Espinosa-Loza, F., Elmer, J. W., Huber, R. Comparison of Cu, Ti and Ta interlayer explosively fabricated aluminum to stainless steel transition joints for cryogenic pressurized hydrogen storage. International Journal of Hydrogen Energy, 2015, 40(3), 1490-1503.

[15] Sherpa, B. B., Upadhyay, A., Kumar, S., Kumar, P. D., Agarwal, A. Examination of Joint Integrity in parallel plate configuration of explosive welded SS-Al combination. Materials Today: Proceedings, 2017, 4(2), 1260-1267.

[16] Banker, J., Nobili, A. Aluminum-steel electric transition joints, effects of temperature and time upon mechanical properties. In: Light Metals, proceedings of 131st TMS Annual Meeting, Seattle, WA, USA, 2002

[17] Nobili, A., Gauthier, D. Specification Number NC 630a. Nobelclad Europe SA, Rivesaltes, France, 2011.

[18] Finnegan, W. D. Steel-to-aluminum transition joint. U.S. Patent No 3,495,319, 1970.

[19] Hofmann, L. Material data sheet: FERAN. Wickeder Westfalenstahl GmbH, Wickede, Germany, 2016

[20] Russo Spena, P. , D'Aiuto, F., Matteis, P., Scavino, G. Dissimilar arc welding of advanced high-strength car-body steel sheets. Journal of materials engineering and performance, 2014, 23(11), 3949-3956.

[21] Russo Spena, P., Matteis, P., Scavino, G. Dissimilar metal active gas welding of TWIP and DP steel sheets. Steel Research International, 2015, 86(5), 495-501.

[22] Cam, G., Ipekoglu, G. Recent developments in joining of aluminum alloys. The International Journal of Advanced Manufacturing Technology, 2017, 91(5-8), 1851-1866.

[23] Gungor, B., Kaluc, E., Taban, E., Aydin, S. I. K. Mechanical and microstructural properties of robotic Cold Metal Transfer (CMT) welded 5083-H111 and 6082-T651 aluminum alloys. Materials and Design, 2014, 54, 207-211.

[24] EN 10346, Continuously hot-dip coated steel flat products for cold forming - Technical delivery conditions. European Committee for Standardization, Brussels, Belgium, 2015

[25] EN 573-3, Aluminium and aluminium alloys - Chemical composition and form of wrought products - Part 3: Chemical composition and form of products. European Committee for Standardization, Brussels, Belgium, 2013

[26] Zhang, H. T., Feng, J. C., He, P., Zhang, B. B., Chen, J. M., & Wang, L. The arc characteristics and metal transfer behaviour of cold metal transfer and its use in joining aluminium to zinc-coated steel. Materials Science and Engineering A, 2009, 499(1-2), 111-113.

[27] ISO 14341, Welding consumables - Wire electrodes and weld deposits for gas shielded metal arc welding of non alloy and fine grain steels - Classification. International Organization for Standardization, Geneva, Switzerland, 2010

[28] ISO 18273, Welding consumables - Wire electrodes, wires and rods for welding of aluminium and aluminium alloys - Classification. International Organization for Standardization, Geneva, Switzerland, 2015.

[29] Gaines, E., Banker, J. Shipboard aluminum/steel welded transition joints: evaluations and improvements. Journal of ship production, 1991, 7(03), 188-199.

[30] ISO/DIS 11845 (draft standard), Corrosion of metals and alloys — General principles for corrosion testing. International Organization for Standardization, Geneva, Switzerland, 2019.

[31] ISO 11845, Corrosion of metals and alloys - General principles for corrosion testing. International Organization for Standardization, Geneva, Switzerland, 1995.

[32] ISO 4136, Destructive tests on welds in metallic materials - Transverse tensile test. International Organization for Standardization, Geneva, Switzerland, 2012.

[33] ISO 6892-1, Metallic materials - Tensile testing - Part 1: Method of test at room temperature. International Organization for Standardization, Geneva, Switzerland, 2016.

[34] ASTM E3, Standard guide for preparation of metallographic specimens. ASTM International, West Conshohocken, United States, 2017.

[35] ASTM E407, Standard practice for microetching metals and alloys. ASTM International, West Conshohocken, United States, 2015.

[36] ISO 6507-1, Metallic materials - Vickers hardness test - Part 1: Test method. International Organization for Standardization, Geneva, Switzerland, 2018.

[37] Ashton, R. F., Wesley, R. P., Dixon, C. R. The effect of porosity on 5086-H116 aluminum alloy welds. Welding Journal, 1975, 54(3), 95s-98s.

[38] Shore, R. J., McCauley, R. B. Effects of porosity on high strength aluminum 7039. Welding Journal, 1970, 49(7), 311s-321s.

[39] Rudy, J. F., Rupert, E. J. Effects of porosity on mechanical properties of aluminum welds. Welding Journal, 1970, 49(7), 322s-336s.

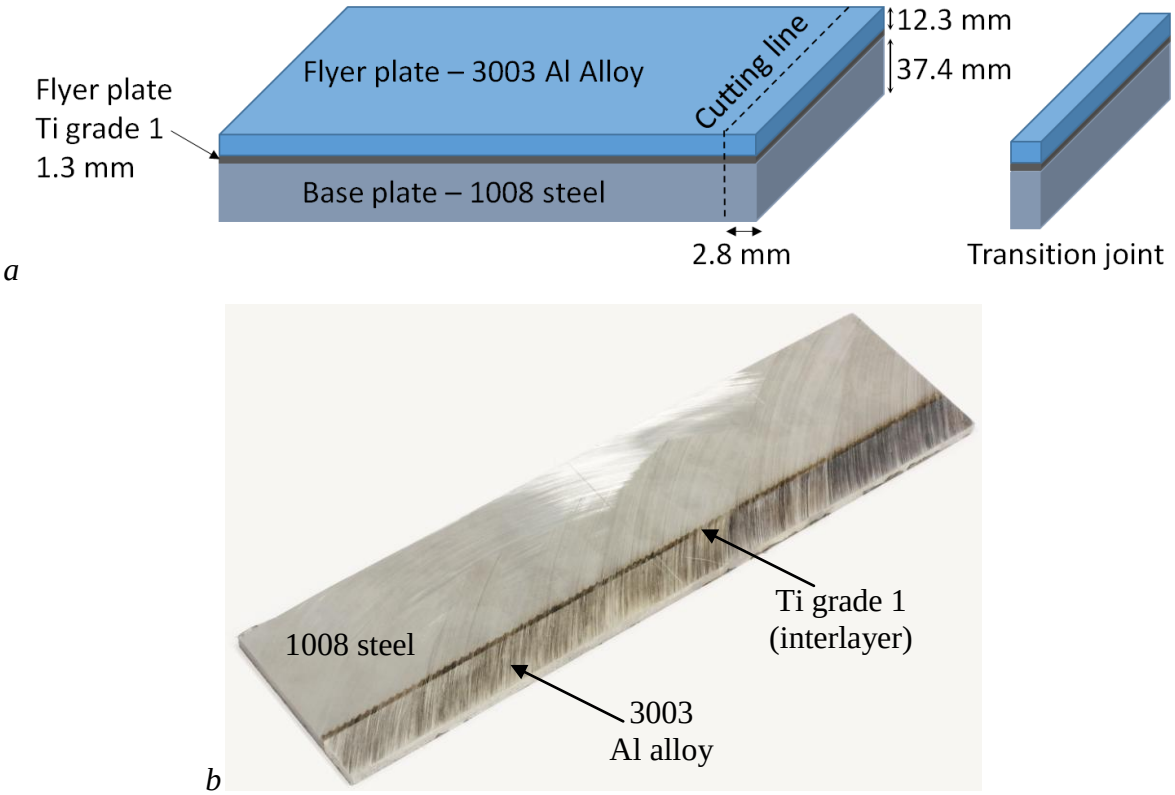

Fig. 1: Sketch of the explosion-welded composite plate and of a transition joint cut from the same plate (a) and picture of one as-cut transition joint (b).

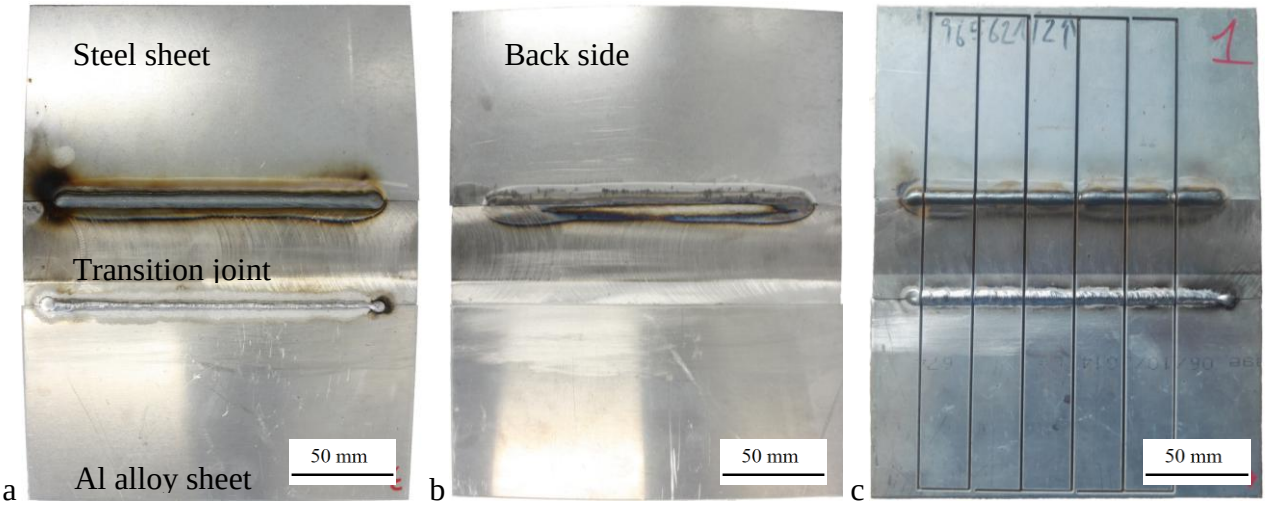

Fig. 2: As welded type B hybrid joint between the 1.35 mm thick DP1000 steel sheet (top) and the 2.5 mm thick 6061 Al alloy sheet (bottom), with the 2.8 mm thick, steel / titanium / Al alloy transition joint between them. View from the torch side (a) and from the back side (b). The same joint, after contour-cutting of 5 transversal tensile specimens by means of abrasive jet milling (c). The sheet width is 200 mm.

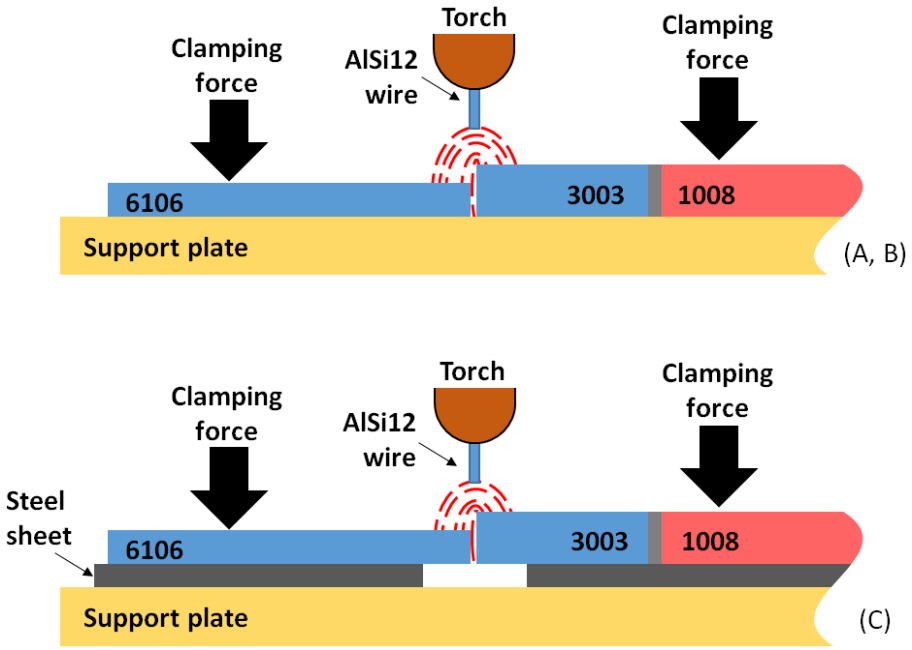

Fig. 3: Schematic welding setup for the aluminum side weld of the type A and B (top) and type C (bottom) hybrid joint specimens.

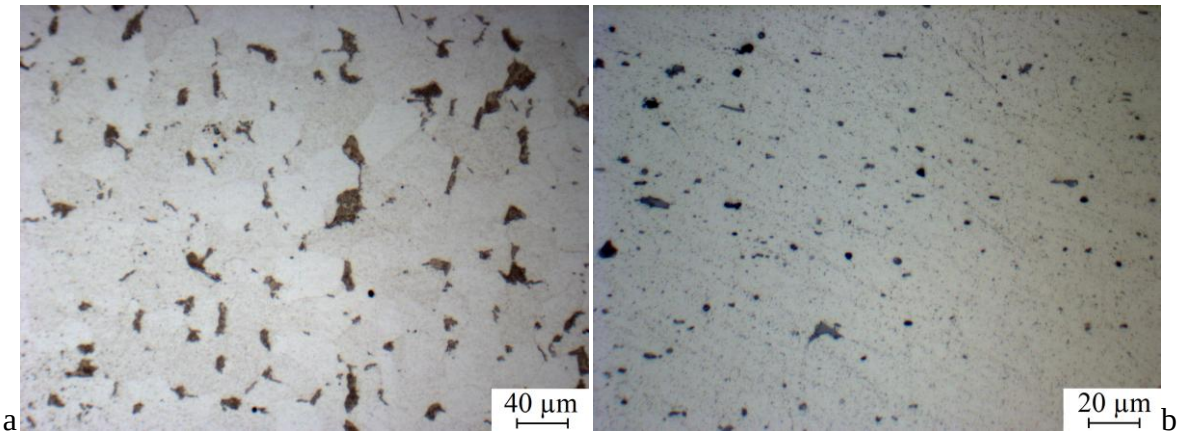

Fig. 4: Microstructure of the DP1000 (batch II) dual phase steel after Nital etching (a) and of the 6106 aluminum alloy after Keller etching (b).

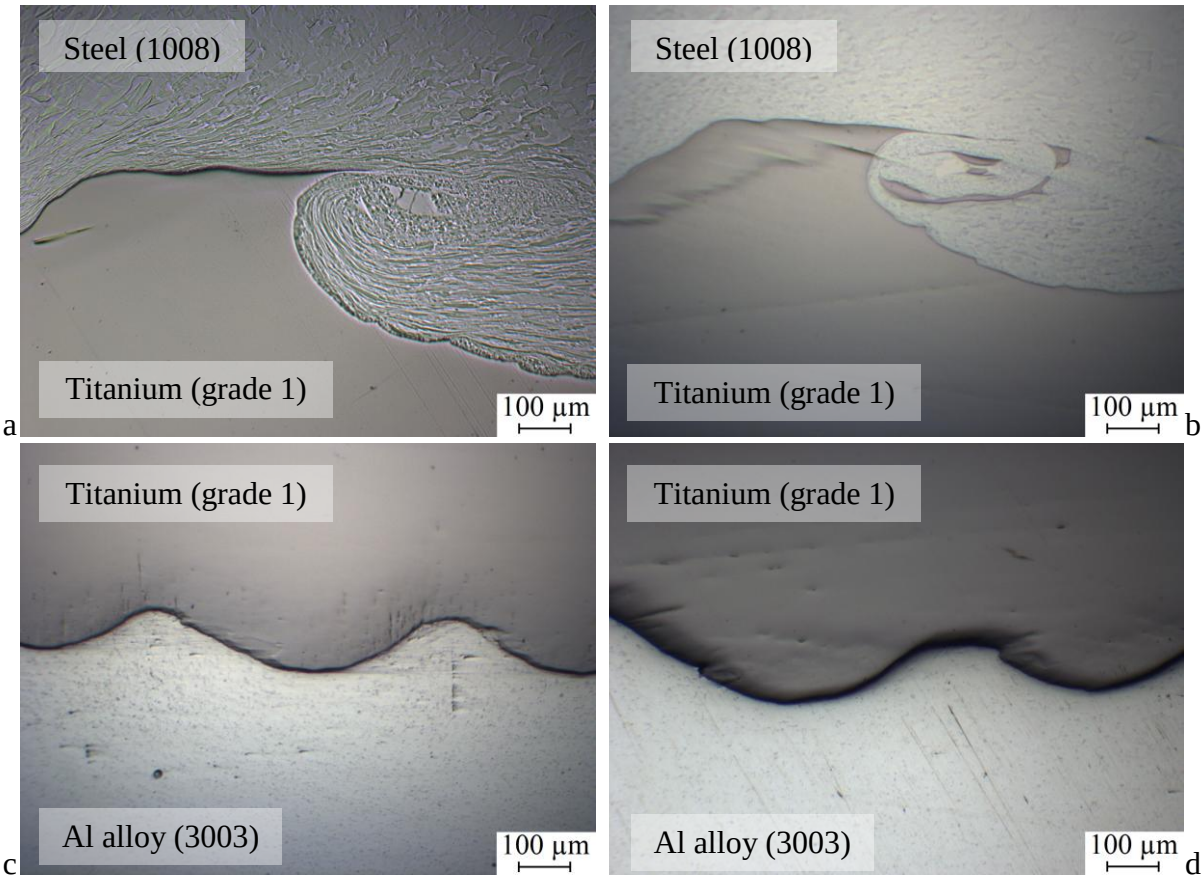

Fig. 5: As-polished cross sections of the explosion welded composite plate, as received (a,c) and after 24 h at 550 °C (b,d). Interfaces between steel and titanium (a,b) and between titanium and Al alloy (c,d).

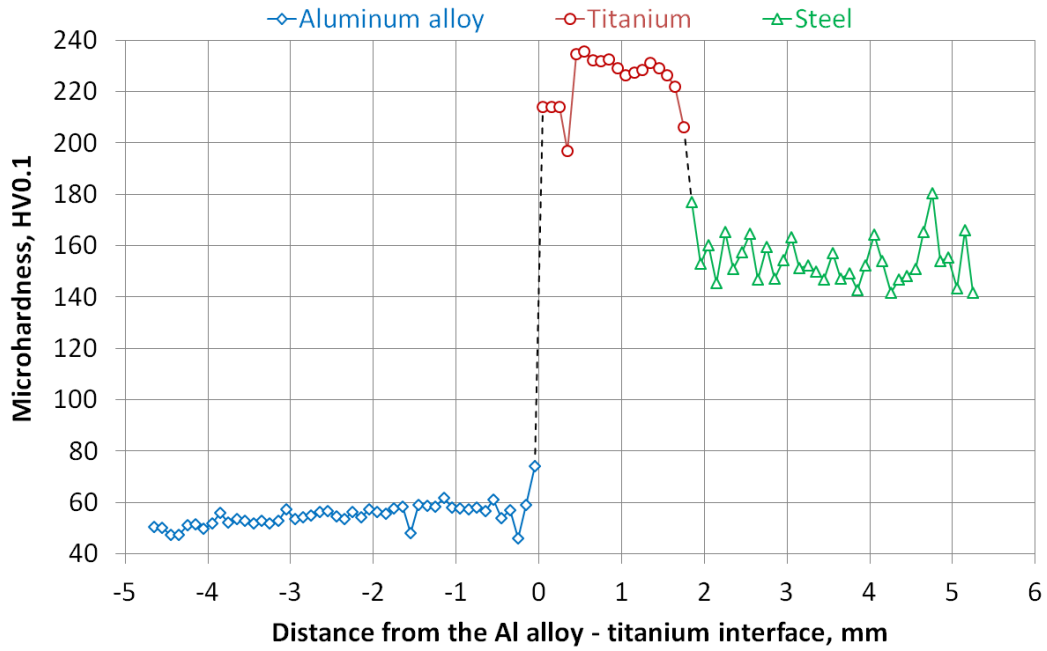

Fig. 6: Microhardness of the explosion welded composite plate, as received, as a function of the distance from the Al alloy - titanium interface.

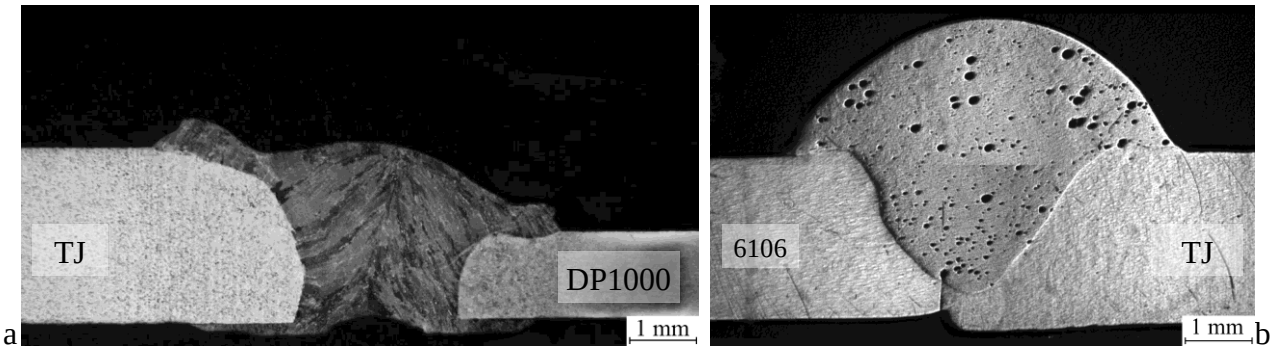

Fig. 7: Cross sections of hybrid joints, showing the weld bead between the transition joint (TJ) and the DP1000 steel sheet in a type C joint (a), and the weld bead between the transition joint and the 6106 Al alloy sheet in a type B joint (b).

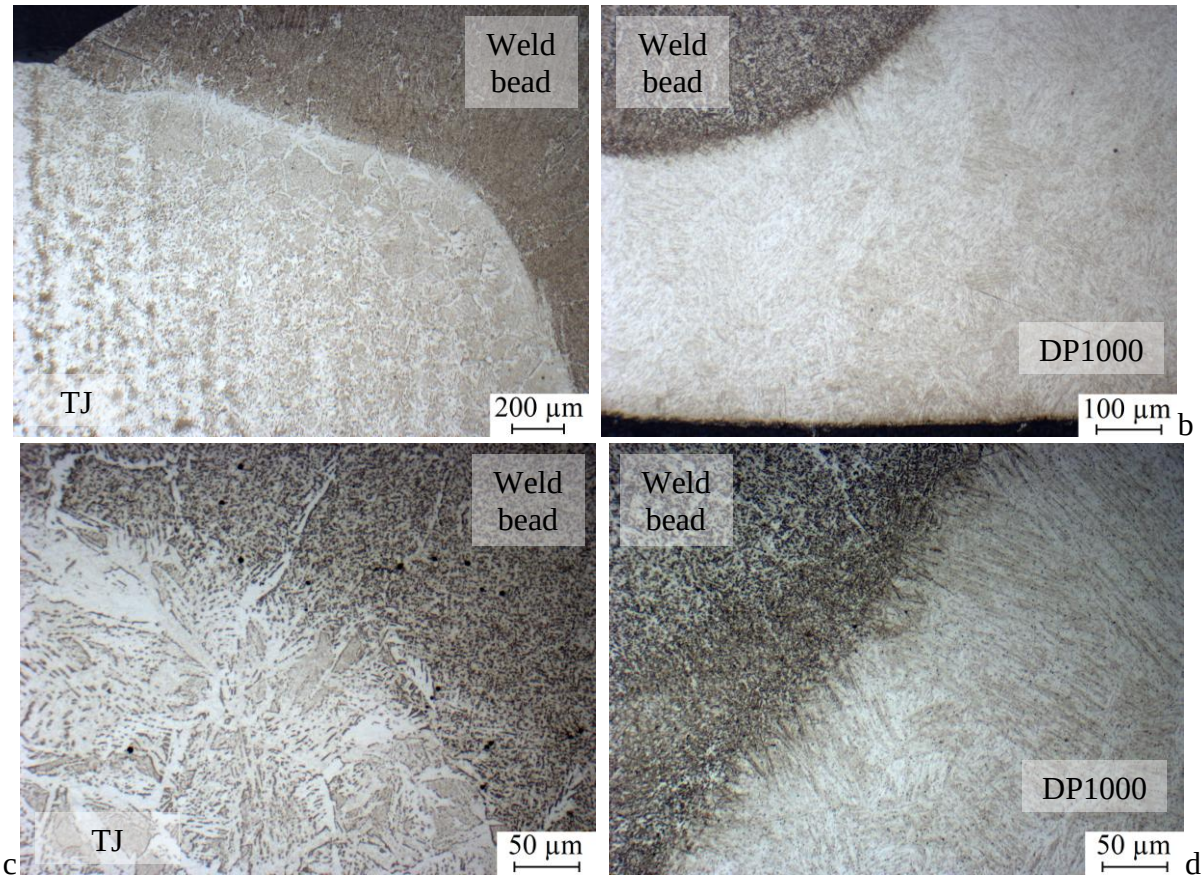

Fig. 8: Cross section of the weld between the DP1000 steel sheet and the steel side of the transition joint. Weld bead (dark) and HAZ on the transition joint side (a,c) and on the sheet side (b,d); increasing magnifications. Type C partial hybrid joint (the Al alloy side was not welded).

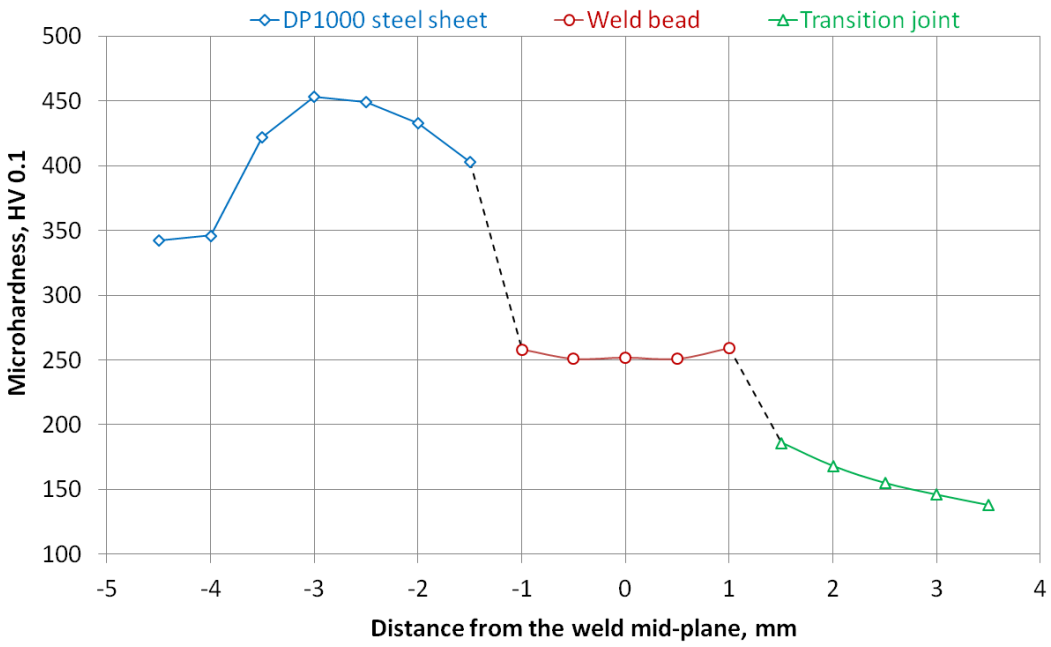

Fig. 9: Microhardness of the weld between the DP1000 steel sheet and the transition joint. Type C hybrid joint.

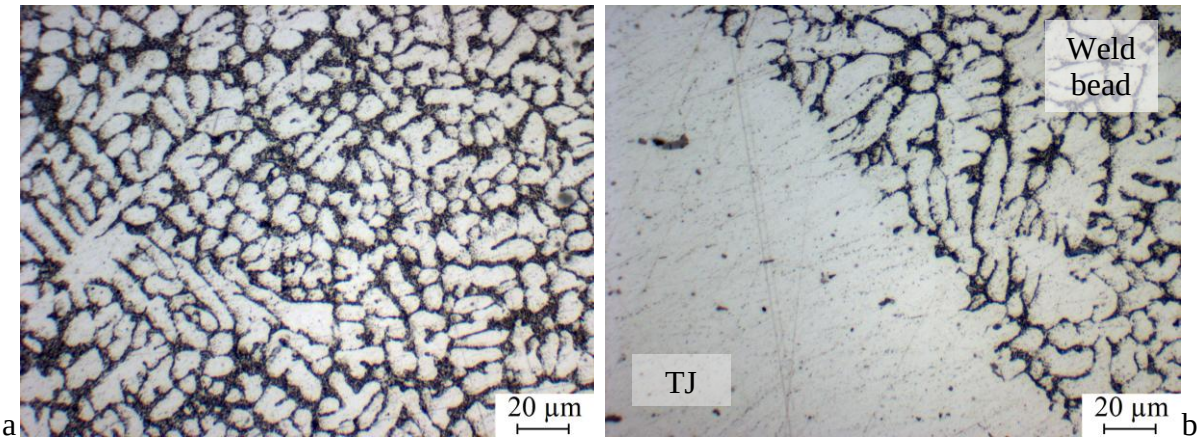

Fig. 10: Cross section of the weld between the 6106 Al alloy sheet and the Al alloy side of the transition joint. Weld bead microstructure (a) and boundary between the weld bead and the HAZ on the transition joint (TJ) side. Type A hybrid joint.

Fig. 11: Microhardness of the weld between the 6106 Al alloy sheet and the transition joint. Type C hybrid joint.

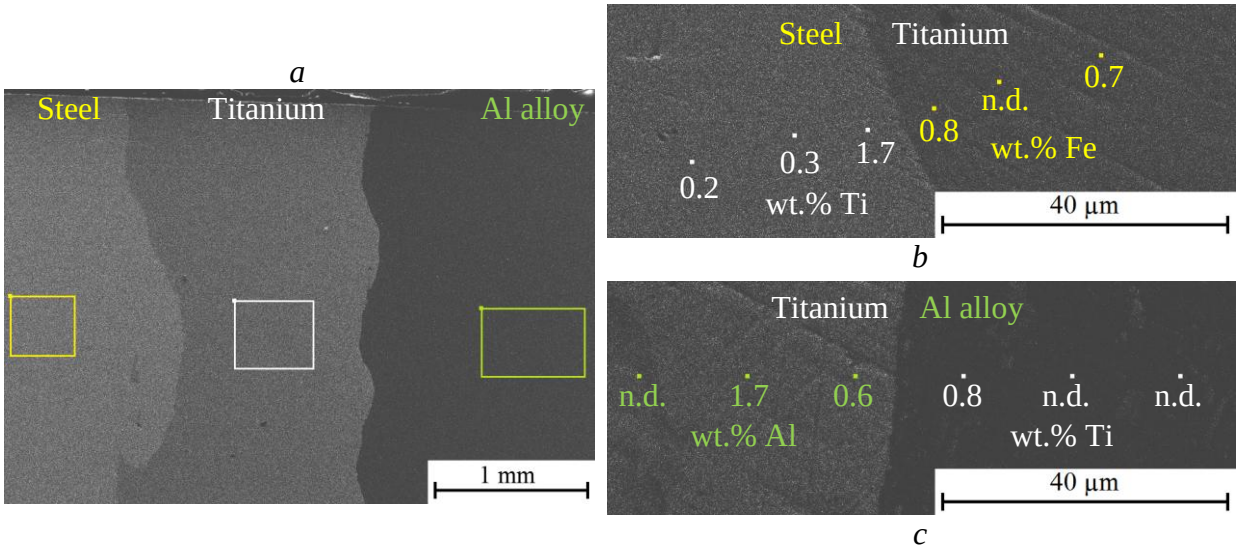

Fig. 12: Cross-section of the transition joint after type B hybrid welding. Overview and EDS analysis areas (boxes, a). Detail of the steel / titanium (b) and titanium / Al alloy (c) interfaces and semi-quantitative results of pointwise EDS analyses (dots) (n.d.: not detected).

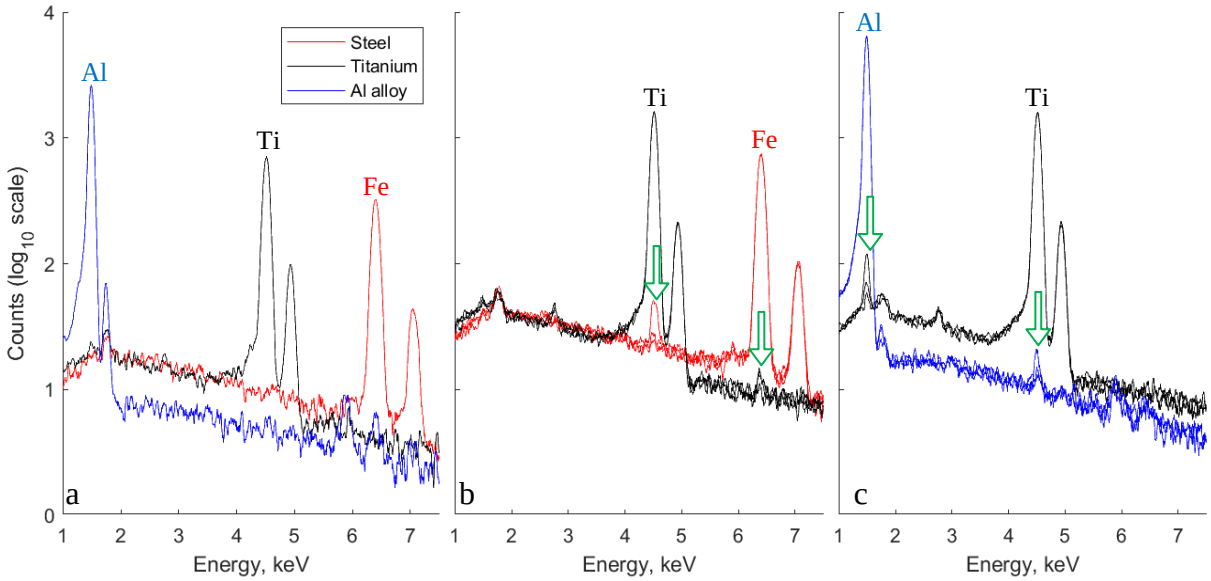

Fig. 13: EDS analyses of the transition joint after type B hybrid welding, in the areas and points shown in figure 12. Area analyses more than 200 µm apart from the welded interfaces (a) and point analyses less than 40 µm apart from the steel / titanium (b) and titanium / Al alloy (c) interfaces Arrows highlight peaks due to interdiffusion. Log scale.

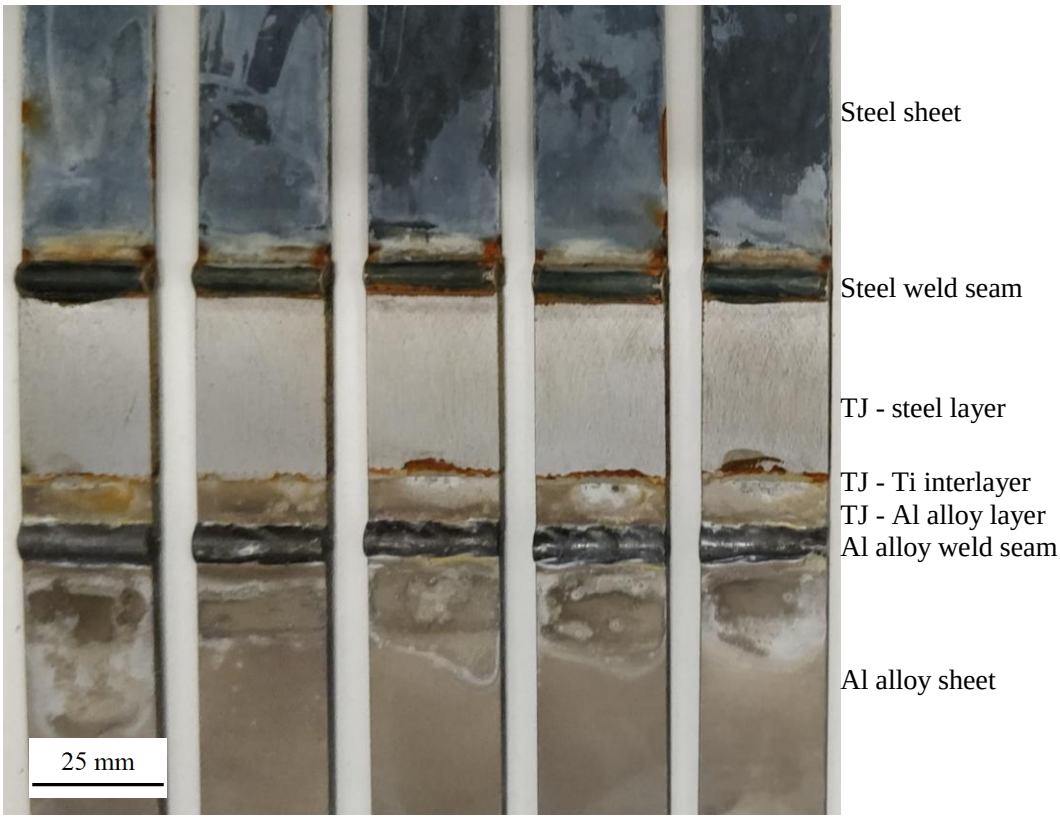

Fig. 14: Type C hybrid joint specimens, after welding and corrosion. The specimens width is 25 mm.

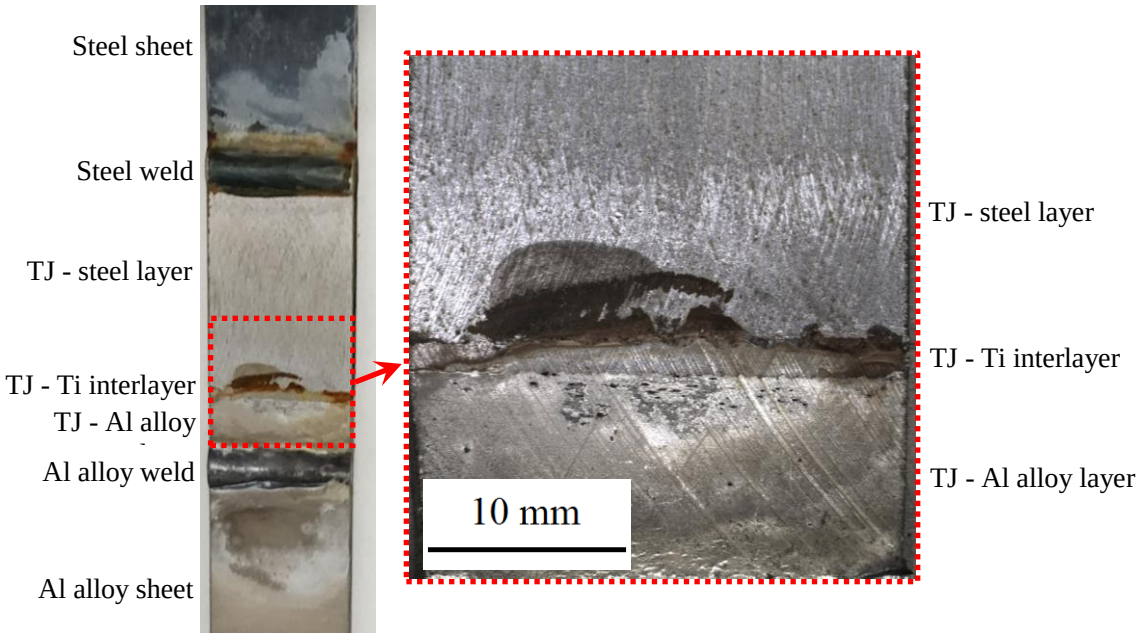

Fig. 15: Type C hybrid joint specimen, after welding and corrosion. Detail of corrosion close to the weld planes of the Transition Joint (TJ). The specimen width is 25 mm.

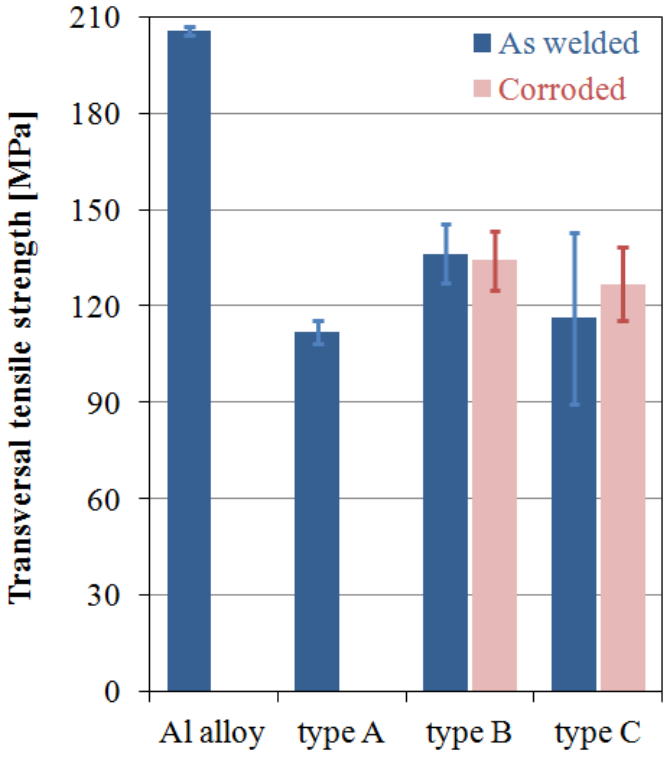

Fig. 16: Transversal tensile strength of homologous and hybrid welded joints.

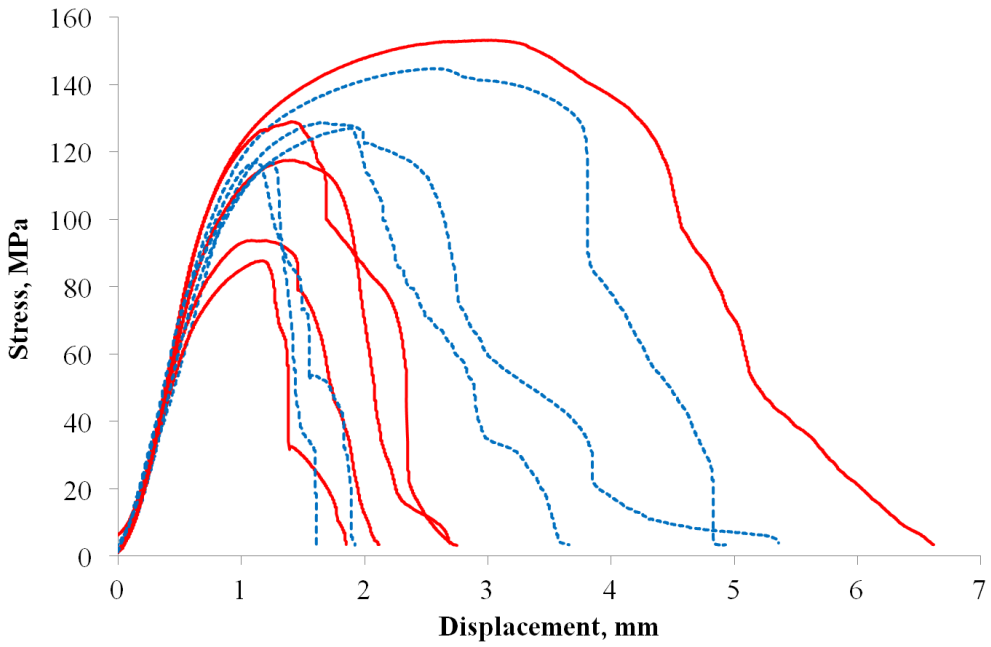

Fig. 17: Tensile test curves of as-welded (continuous lines) and corroded (dotted lines) type C hybrid joint specimens. The stress is calculated on the basis of the initial cross section of the Al alloy sheet.

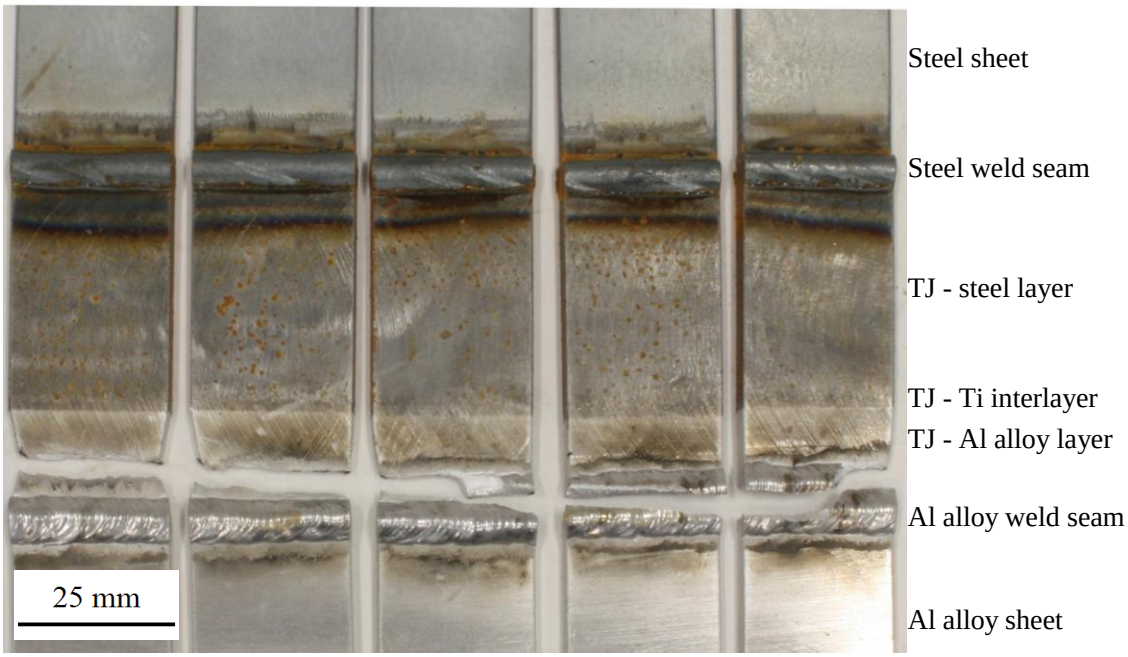

Fig. 18: Type B hybrid joint specimens, after welding and tensile testing. TJ means Transition Joint.

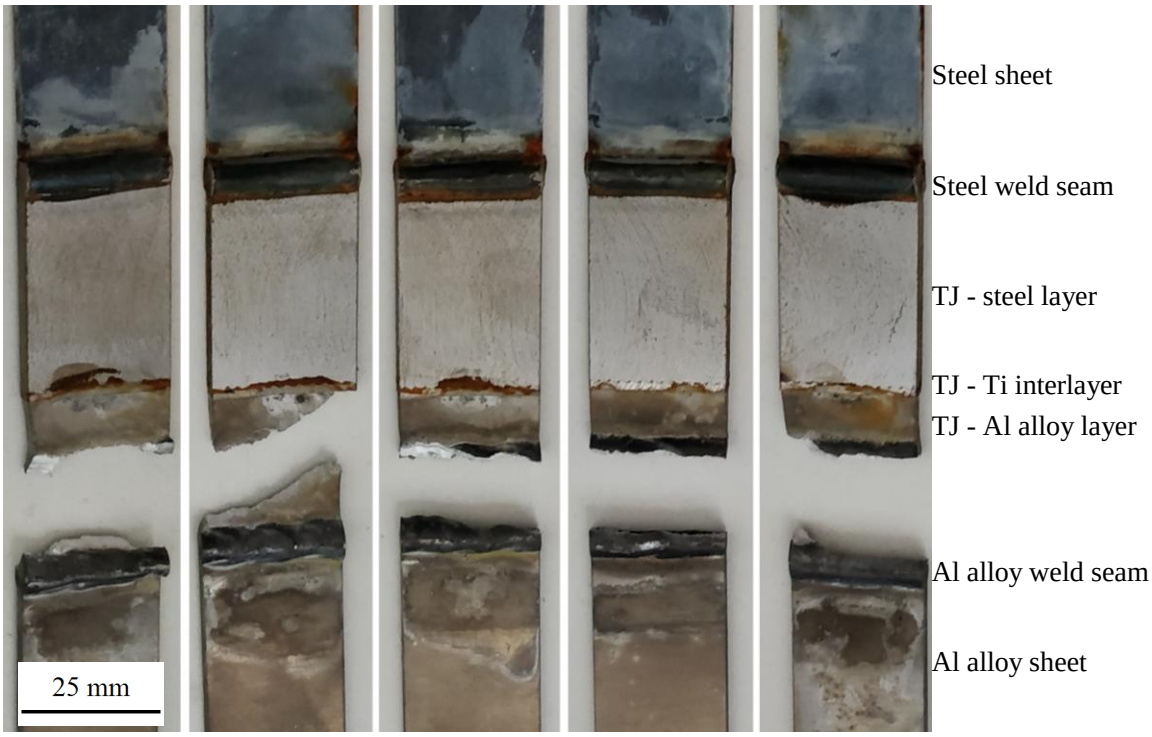

Fig. 19: Type C hybrid joint specimens, after welding, corrosion, and tensile testing. TJ means Transition Joint.

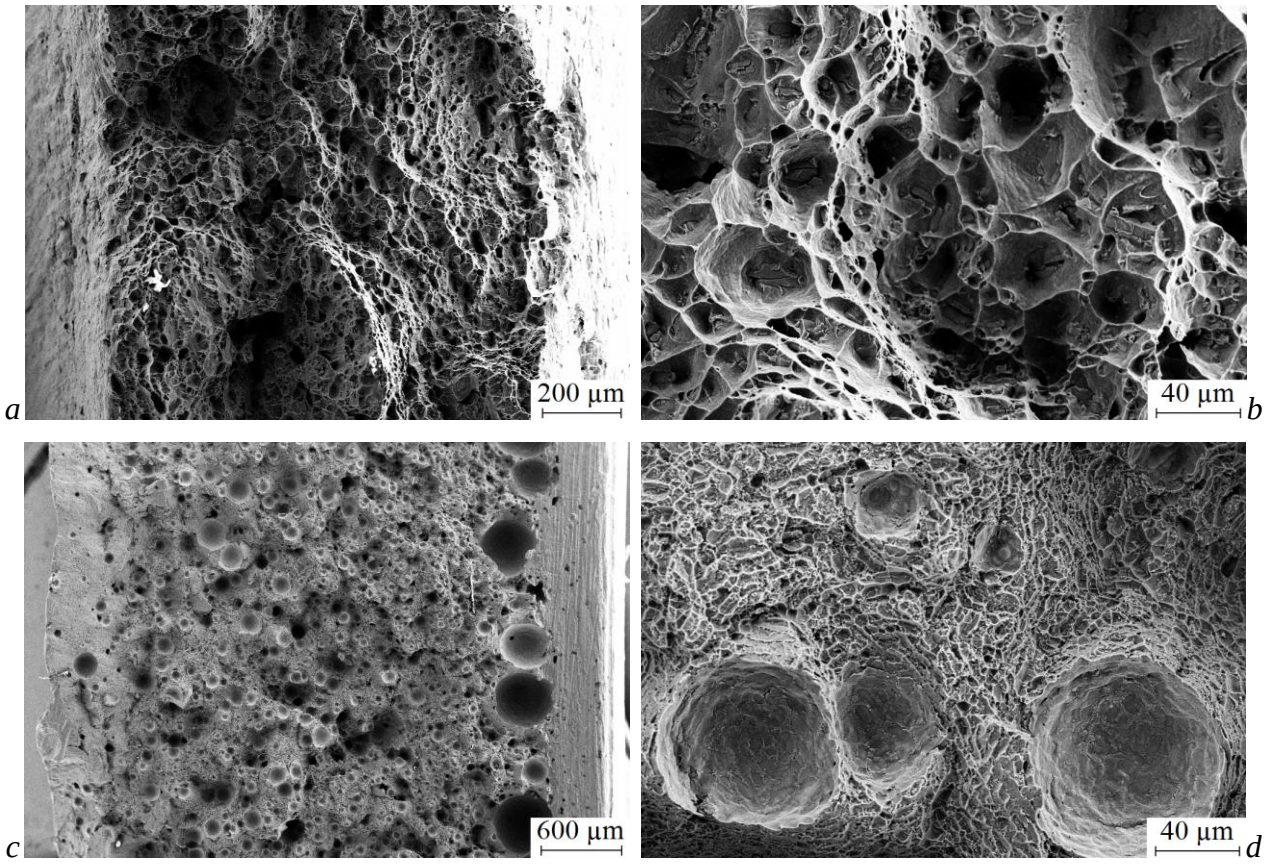

Fig. 20 - Fracture surfaces of transversal tensile specimens obtained from type B hybrid joints. Specimens broken in the HAZ of the transition joint, close to the Al-alloy weld seam (a,b) and in the Al-alloy weld seam (c,d); full-thickness view (a,c) and detail (b,d).

Table I - Arc-welding tests. Steel batch, type of joints, number of welding tests and of ensuing tensile specimens, and selected process parameters for the steel and Al alloy welds.

Type of welded joint		Steel batch	Tests	Specimens	Steel weld				Al alloy weld			
					Wire speed mm/s	Torch speed mm/s	Arc current A	Arc tension V	Wire speed mm/s	Torch speed mm/s	Arc current A	Arc tension V
Homologous	steel	I	1	4	38	7.7	71	20	-	-	-	-
	Al alloy	-	1	5	-	-	-	-	92	7.7	115	13.5
Hybrid	type A	I	1	4	53	7.7	115	16	53	4.7	48	15.5
	type B	I	2	10	53	7.7	115	16	75	7.7	71.5	15
	type C	II	2	10	53	7.7	115	16	100	7.7	115	13

Table II - Chemical composition of the examined steels

Steel	Batch	C	Si	Mn	P	S	Al	Cr	Mo	Ni	Cu	Nb	Ti	V	B
DP1000	I	0.13	0.17	2.2	0.009	0.003	0.043	0.45	0.017	0.016	0.014	0.026	0.004	0.003	0.001
	II	0.14	0.18	2.2	0.009	0.002	0.046	0.46	0.016	0.017	0.015	0.028	0.004	0.003	0.001
1008	-	0.069	0.18	0.44	0.014	0.0007	0.031	0.045	0.006	0.037	0.024	n.a.	n.a.	n.a.	n.a.

Table III - Chemical composition of the examined aluminum alloys

Alloy	Si	Fe	Cu	Mn	Mg	Cr	Ni	Zn	Ti
6106	0.59	0.24	0.092	0.13	0.61	0.030	0.005	0.033	0.012
3003	0.20	0.57	0.085	1.3	0.0057	0.0018	0.004	0.0065	0.021

Table IV - Transversal tensile strength of homologous and hybrid welded joints. The strength is calculated on the basis of the initial sheet cross section; for hybrid joints, the Al alloy sheet cross-section is used.

Type of welded joint		Transversal tensile strength (MPa)					
		As welded			Corroded		
		Tests	Mean	St. Dev.	Tests	Mean	St. Dev.
Homologous	steel	4	763	207	-	-	-
	Al alloy	5	206	1	-	-	-
Hybrid	type A	4	112	4	-	-	-
	type B	5	136	9	5	134	9.2
	type C	5	116	27	5	127	11.5